Surface & Coatings Technology 358 (2019) 435–442

Contents lists available at ScienceDirect

Surface & Coatings Technology

journal homepage: www.elsevier.com/locate/surfcoat

# Improving the interaction between aluminum surfaces and polymer coatings

Lisa Muñoz[a,*], Fabiola Pineda[c], Carola Martínez[b,d], Mamié Sancy[b], Marcela Urzua[e], Marcos Flores[f], María V. Encinas[g], Maritza A. Páez[a]

[a] Departamento de los Materiales, Facultad de Química y Biología, Universidad de Santiago de Chile, Alameda 3363, Estación Central, Chile
[b] Escuela de Construcción Civil, Pontificia Universidad Católica de Chile, Vicuña Mackenna 4860, Santiago, Chile
[c] Escuela de Ingeniería, Pontificia Universidad Católica de Chile, Vicuña Mackenna 4860, Santiago, Chile
[d] Instituto de Química, Pontificia Universidad Católica de Valparaíso, Av. Universidad 330, Valparaíso, Chile
[e] Departamento de Química, Facultad de Ciencias, Universidad de Chile, Las Palmeras 3425, Ñuñoa, Santiago, Chile
[f] Departamento de Física, Facultad de Ciencias Físicas y Matemáticas, Universidad de Chile, Beauchef 850, Santiago, Chile
[g] Departamento Ciencias del Ambiente, Facultad de Química y Biología, Universidad de Santiago de Chile, Alameda 3363, Estación Central, Chile

ARTICLE INFO

*Keywords:*
Argon-plasma treatment
Coating
Poly(methyl methacrylate)
Surface
Aluminum alloy

ABSTRACT

To better understand the effect of surface treatments on the efficiency of protective coatings of aluminum alloys, this study assessed different surface treatments for the aluminum alloy AA2024, including mechanical polishing, chemical etching and Ar-plasma pretreatment followed by deposition of poly(methyl methacrylate). Surface morphology, surface chemical analysis and wettability of the treated samples were characterized by scanning electron microscopy, X-ray photoelectron spectroscopy and contact angle, respectively. Open circuit potential and electrochemical impedance spectroscopy were carried out in a 0.1 M solution of $Na_2SO_4$ as a function of exposure time. SEM images revealed that a homogeneous and well incorporated poly-(methyl methacrylate) coating was obtained by using Ar-plasma as a pretreatment. XPS spectra showed that the Al—O/Al—OH intensity ratio of the Ar-plasma pretreated samples does not show clear dependence on angle measurement, which indicates that Al(OH) and $Al_2O_3$ are not homogenously distributed on the sample surfaces. $Al_2O_3$ does not completely cover the aluminum surface, leaving some areas exposed. The measurements of the hysteresis angle showed that the Ar-plasma pretreatment favors chemical heterogeneity, which in turn increases the hydrophilicity of the coated samples, resulting in lower wettability and a greater hysteresis angle. The electrochemical results showed that the Ar-plasma pretreatment significantly improves the protective capacity of poly(methyl methacrylate).

## 1. Introduction

Chromate anodizing has been used widely as an anti-corrosive surface treatment with light alloys like those of aluminum. However, the high degree of toxicity and carcinogenic effects related to $Cr^{+6}$ species have made their use unacceptable and chromate-free pretreatments are being developed [1,2]. Research on anticorrosion treatments of aluminum alloy (AA) surfaces have involved different organic coatings that have shown the fundamental role of pretreatment in providing effective protection. Numerous mechanical, chemical, electrochemical and other surface treatments to improve the durability of aluminum alloys have been studied, such as liquid or vapor degreasing, abrading, grit blasting, acid/alkaline etching and anodizing. N. Saleema et al. [3] reported that NaOH treatment improves metal-coating interaction. Tiringer et al. [4] demonstrated that treatment with NaOH produces a rough layer on the surface of AA2024-T3, with complete removal of intermetallic particles. Other surface treatments have shown that functionalization with silane improves the performance of the metal surface [5,6]. Luciano et al. [6] studied the protective capacity of novel eco-friendly hybrid epoxy–silicon (EP-S) coatings to prevent the corrosion of AA after exposure to NaCl in solution, and found that functionalizing the coating improves the protection of the metal.

Pretreatments using plasma have attracted attention because they can: (i) improve the removal of organic contaminants from surfaces that can interfere with adhesion, (ii) cause micro-etching that increases surface area, (iii) remove weak boundary layers, (iv) and modify surface chemistry resulting in improved chemical and physical interactions at the bonding interphase. Pretreatment using plasma can favor the formation of free-radicals and atomic or molecular fragments, which influences the formation of volatile species that can be removed by the

* Corresponding author.
*E-mail address:* lisa.munozm@usach.cl (L. Muñoz).

https://doi.org/10.1016/j.surfcoat.2018.11.051
Received 11 July 2018; Received in revised form 16 November 2018; Accepted 18 November 2018
Available online 23 November 2018
0257-8972/ 

**Table 1**
Sample nomenclature.

| Sample | Nomenclature |
|---|---|
| AA2024-T3 treated with mechanical polishing and chemical etching | T |
| AA2024-T3 with mechanical polishing, chemical etching and Ar-plasma surface treatment | T-ArP |
| AA2024-T3 with mechanical polishing, chemical etching and polymeric coating | T-PMMA |
| AA2024-T3 with mechanical polishing, chemical etching, Ar-plasma surface treatment and polymeric coating | T-ArP-PMMA |

The electrochemical measurements were repeated in duplicate and the other measurements in quadruplicate.

vacuum system. These can either react to produce cross-linking of the surface or even the ground state molecules, possibly forming new chemical species on the surface. Inert gases like Ar or He are used to generate free radicals on surfaces, either to cause crosslinking, or to leave active sites for later reaction with a purge gas. Hence, if the plasma is an inert gas like argon or helium, the surface may contain a large number of stable radicals that can persist even after exposure to a reactive gas. These gases should not be used alone for cleaning because there is no mechanism for converting the molecular fragments to permanently volatile compounds. Therefore, the fragments polymerize or reposition [7,8].

Mui et al. [9] proposed that modifying an AA surface by atmospheric pressure plasma treatments improves the corrosion resistance of polyurethane-coated AA7075. In effect, the adhesion and efficiency of anticorrosion coatings for metal alloys is an important issue that is largely determined by the surface treatment, the chemical composition of the alloy and the composition of the organic coating [10,11].

Hydroxyl groups on a metallic surface can modify the physicochemical properties of that surface. McCafferty et al. [10] estimated the surface concentration of hydroxyl groups in metals coated with oxide film by using the treatment with argon plasma, revealing that this type of pretreatment reduces the thickness of the contaminant layer without altering the aluminum-intermetallic particle ratio [12]. Giza et al. [13] showed that for extremely short periods of time the plasma treatment changes the chemical composition of the surface and the kinetics of incorporating a monolayer, thus increasing surface hydroxyl density. Grundmeier et al. [14] showed that the chemistry of the surface and the thickness of the oxide of the coated iron alloy are modified after treatment with oxygen plasma. In particular, the plasma pretreatment represents an efficient, non-polluting and economic alternative to increase the adhesive properties of an aluminum surface coating [15–19] to which subsequent coatings can be applied [8,9].

In this study, an argon-plasma pretreatment was applied to AA2024-T3 samples prior to the application of poly(methyl-methacrylate) (PMMA). The effect of the pretreatment was assessed by contact angle measurements, scanning electron microscopy and electrochemical techniques.

## 2. Experimental details

### 2.1. Metal samples

The aluminum alloy 2024-T3 (ENAER, Empresa Nacional de Aeronáutica de Chile) was used as the working electrode, with the following chemical composition (wt%): 92.400 Al, 4.900 Cu, 1.520 Mg, 0.169 Fe, 0.520 Mn, 0.085 Si. The samples consisted of 100 × 100 × 1.8 mm plates machined from an AA2024-T3 rolled plate.

### 2.2. Synthesis of the poly(methyl methacrylate) coating (PMMA)

The polymer was formed by mixing 20 mL of methyl methacrylate (MERCK, 99%, stabilized. 186.98 mmol; d = 0.936 g/mL; PM. 100.12 g/mol), previously washed with 5% NaOH, dried with calcium hydride ($CaH_2$) and finally distilled and polymerized with 0.02 g of benzoyl peroxide (MERK, 75%. 0.08 mmol; d = 1.334 g/mL; PM = 242.23 g/mol) under magnetic stirring for 90 min at 55 °C. All chemical reagents were purchased from Merck and used without further purification.

### 2.3. Surface treatment

#### 2.3.1. Surface pretreatment

The metal samples were polished with silicon carbide paper (from #400 to #4000 grade) and degreased with acetone, washed with bidistilled water and dried under air flow. The samples were then activated by the following procedure: immersion for 2 min in 0.1 M of a NaOH solution, washing in water, immersion in 20% v/v $HNO_3$ solution for 5 min, washing in water and ethanol, following which the samples were dried for 30 min at room temperature.

#### 2.3.2. Argon plasma cleaning

Some metal samples received an additional surface pretreatment of an Ar-plasma flow applied with a Plasma Prep III device that consisted of a RF power supply (13.56 MHz) in a dielectric quartz tube in a hollow electrode. The gas flowing out of the nozzle formed a plasma jet of pure Ar (5 L/min). The power applied to the electrode was adjusted to 80 W for 120 s at a pressure of 170 mtorr. The samples were immersed in a polymer solution for 6 min and then air dried.

Table 1 gives the nomenclature used for the samples:

### 2.4. Surface analysis techniques

The morphology of the metal samples was investigated by scanning electron microscopy (SEM) using TESCAN S8000 at an acceleration voltage of 5 kV. Cross sections of the coated samples were obtained by ultramicrotomy to characterize the surface-coating interface. The surface composition of the samples was studied with X-ray photoelectron spectroscopy (XPS). XPS spectra were collected using a PHI1250 photoelectron spectrometer (Physical Electronics) with an Al $K\alpha$ X-ray source ($h\nu$ = 1486.71 eV). To minimize ageing and contamination effects, samples were stored in a nitrogen atmosphere, beginning no more than an hour after preparation. The analysis chamber operated in a vacuum at lower than $1 \times 10^{-6}$ mbar while measurements were made. After a survey scan, high-resolution scans of the O1s, N1s, C1s and Al2p signals were recorded at take-off angles that ranged from 0 to 75°, using pass energy of 44.75 and 0.2 eV step size. X-ray photoelectron spectroscopy data were analyzed with PHI Multipak software (V9.4.0.7). The energy scale of the spectra were calibrated relative to the binding energy (BE) of advantageous hydrocarbons (C—C/C—H) in the C1s signal at 284.8 eV. Curve fitting and decomposition were performed after Shirley-type background removal. A mixed Gauss–Lorentz shape was used for the different components.

### 2.5. Contact angle and water absorption

The contact angle measurements of the samples were determined by the sessile drop or static drop method at 25 °C using a contact angle device (Drop Shape Analyzer DSA25S, KRUSS) controlled by ADVANCE software (KRUSS). Eight microliter drops of water or diiodomethane were deposited on the surfaces. Drops of sessile water of 8 and 4 μL

were used for advancing (θa) and receding contact angle (θr), respectively, obtaining the hysteresis in the contact angle, which is the difference between the angle advance and the angle reced ($\Delta\theta = \theta a - \theta r$).

### 2.6. Electrochemical measurements

A three-electrode electrochemical cell was used for electrochemical measurements. Metal samples were employed as working electrodes with an exposed surface area of approximately 15 $cm^2$. A 0.1 M solution of $Na_2SO_4$ (reagent grade) was used as an electrolyte. A graphite rod and a saturated calomel electrode were used as counter and reference electrodes, respectively. The electrochemical cell was kept at room temperature and open to the air. Open circuit potential and electrochemical impedance measurements were carried out using a Bio-Logic VSP. Impedance diagrams were obtained over a frequency range from 100 kHz to 3 mHz, with eight points per decade using a 10 to 70 mV peak-to-peak sinusoidal voltage at E = OCP. The linearity of the system was checked by varying the amplitude of the ac signal applied to the sample. The electrochemical behavior was characterized as a function of immersion time.

## 3. Results and discussion

### 3.1. Surface characterization

#### 3.1.1. SEM analysis

Fig. 1 shows the SEM images of the cross sections of the T-PMMA and T-ArP-PMMA samples. In both cases, there are smooth compact PMMA layers with thicknesses of 20 and 25 μm, respectively. Fig. 1(b) revealed a further improvement of the PMMA/AA interface by Ar-plasma surface pretreatment, which indicates the activator effect of the supplementary Ar-plasma treatment on the alloy surface, facilitating better anchoring of the PMMA.

#### 3.1.2. XPS analysis

In the present study, the binding energy was corrected by using the main C1s signal peak at 284.8 eV as a reference, but prior to calibrating the energy, no differences in the charge effect of T and T-ArP were observed. Regarding the Al2p signal, Fig. 2 shows the XPS spectra of the T and T-ArP samples for different take-off angles. Two main peaks of this signal were identified, at 72.3 ± 0.1 eV and 74.9 ± 0.1 eV, corresponding to $Al^0$ and $Al^{3+}$, respectively. The $Al^0$ peak (metallic) was always less intense than that of $Al^{3+}$ (oxide film) in both samples. In fact, the intensity of the metallic peaks decreases as the take-off angle increases. This is more evident in the graph, which shows the dependence of the $Al^{3+}/Al^0$ intensity ratio on the take-off angle Fig. 2(c, d). Oxide thickness can by estimated by fitting the experimental data on this graph. The aluminum oxide thicknesses are 4.0 nm and 3.5 nm for the T and T-ArP samples, respectively.

The Al2p signal only gives information about oxide film was formed spontaneously on cleaned aluminum surfaces. Valuable understanding of the mixed oxide formed in the interfase can be gained from studying ARXPS, including the O1s signal [20]. In the present study, the two main contributions of the O1s signal were identified at 532.3 ± 0.1 eV and 534.7 ± 0.1 eV (Fig. 3(a, b)), corresponding to Al—O and Al—OH, respectively [21]. Fig. 3(c) shows that for T and T-ArP samples, the Al—O/Al—OH intensity ratio depends on the take-off angle. Dependence on the angle was observed in chemically cleaned samples, which indicates that the Al—OH is on the Al—O, or that Al—OH is, as expected, on the outermost surface. However, with samples treated with Ar-plasma, the Al—O/Al—OH intensity ratio does not show clear dependence on the angle, which indicates that Al(OH) and $Al_2O_3$ are not homogenously distributed on the surface of the sample Fig. 3(d) shows $Al_2O_3$ does not fully cover the aluminum surface and some areas of Al (OH) are exposed.

#### 3.1.3. Contact angle measurements

Table 2 shows the contact angle and surface energy data of the T, T-ArP, T-PMMA and T-ArP-PMMA samples in water and diiodomethane. As can be seen in Table 2, the forward angle for the T sample was nearly 57° and 49° in water and diiodomethane, respectively. The contact angle of the T-ArP sample decreased to 18° in water, and from 49° to 44° in diiodomethane, as shown in Table 1. The contact angles of the coated samples did not show the effect of the Ar-plasma pretreatment. However, differences associated with surface roughness, area and chemical composition, which can influence the hydrophobicity of the surface, were better evidenced by estimating the hysteresis angles (Fig. 4). Mrad et al. [22] determined that an increase in the hydrophilic surface improves wettability with organic compounds with polar groups since it increases hydroxyl groups, this is in accordance with the results of XPS presented in Fig. 3. For T-PMMA and T-ArP-PMMA samples, the advancing angles (θa) were 79.1 ± 0.2° and 89.8 ± 0.2°, respectively (Fig. 4(c1, d1)), which can be attributed to an increase in hydrophobicity. This suggests that the PMMA adsorbed on the aluminum surface pretreated with Ar-plasma has more affinity and that the polar groups are oriented toward the metal-coating interface, leaving groups that are more apolar oriented outwardly [12,22–24]. This is in agreement with the high degree of chemical heterogeneity among the samples, as was estimated by the higher hysteresis value (Δθ) of 29.3 ± 0.3° than 19.4 ± 0.2° (Fig. 4(c, d)) and can also be seen in the SEM cross section images shown in Fig. 1.

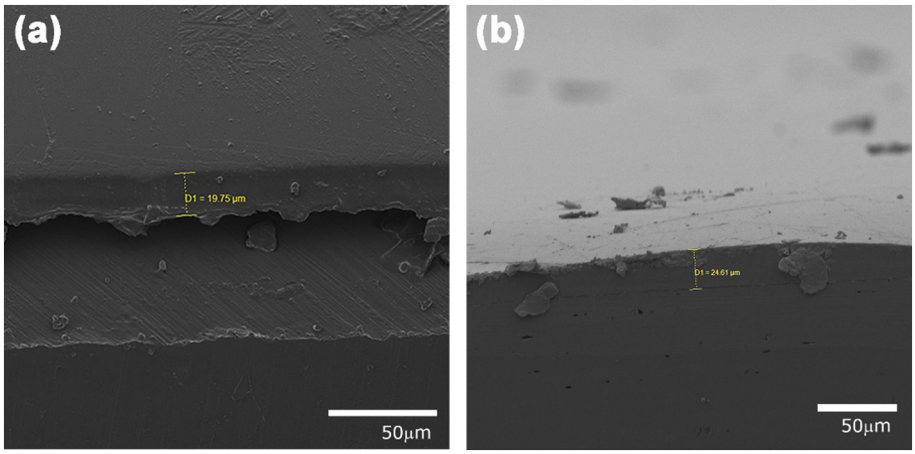


**Fig. 1.** SEM images of cross-section of the (a) T-PMMA and (b) T-ArP-PMMA samples before exposure to 0.1 M $Na_2SO_4$ solution.

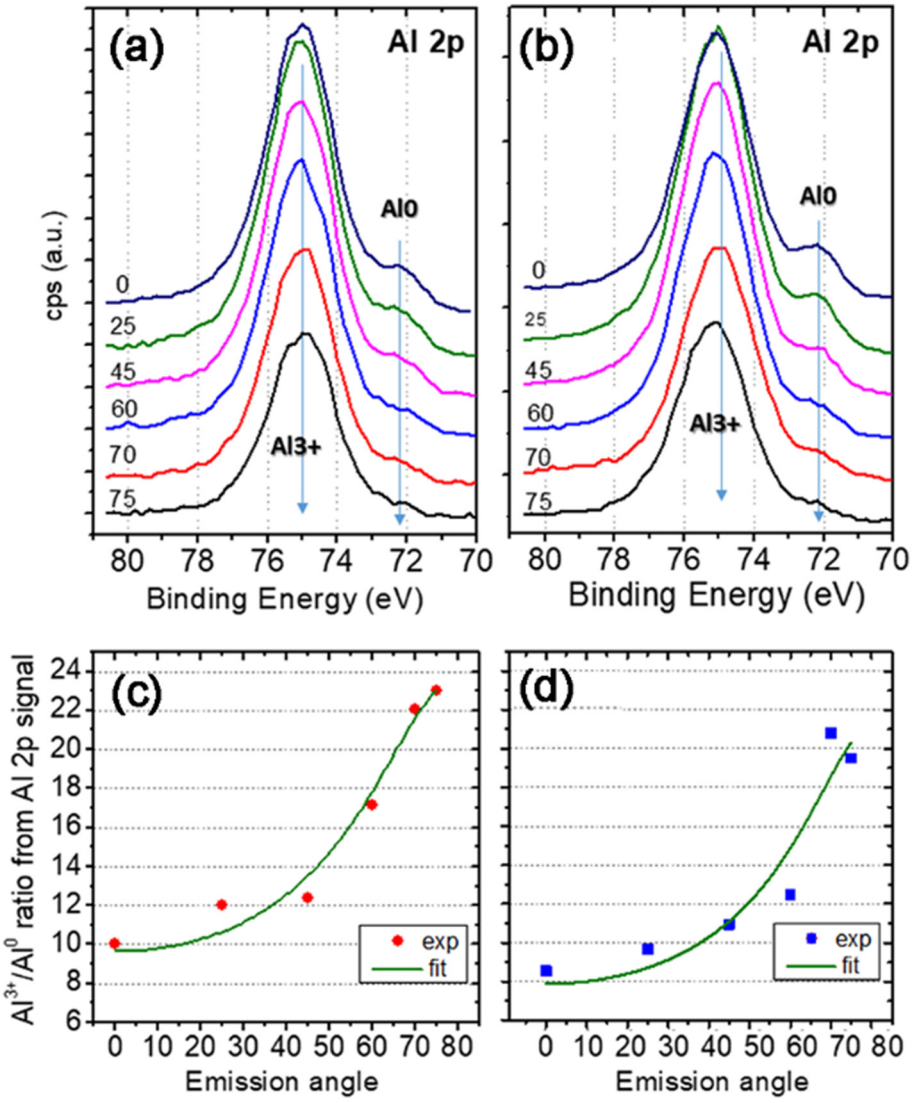


**Fig. 2.** XPS spectra of Al2p signal and $Al^{3+}/Al^{0}$ intensity ratios measured at different take-off angle for (a, c) T and (b, d) T-ArP samples.

### 3.2. Electrochemical results

Fig. 5 shows the Bode plots of the T sample after exposure to a 0.1 M solution of $Na_2SO_4$ at E = OCP, which consisted of a capacitive loop associated with the cathodic part of impedance, in parallel with the anodic part. In this case, the anodic part was related to charge transfer resistance ($R_{ct}$) associated with oxide film formation on the aluminum surface, while the cathodic part may be related to the oxygen-reduction reaction on the intermetallic particles and the oxide film. The modulus values (|Z|) at the low frequency range (LF) correlate with oxide film resistance (Fig. 5(a)), which increased slightly with time, indicating a slight fall in the anodic current, as shown in Table 3. The variation in the phase angle (θ) as a function of exposure time reveals CPE behavior at the middle frequency range (Fig. 5(b)), with θ values around 75°. CPE fit parameters α and Q are given in Table 3. α values were around 0.85 for the entire exposure time and the Q coefficient increased slightly with time from $2.1 \times 10^{-6}$ to $2.8 \times 10^{-6}\,s^{-\alpha}\,cm^2$. The slight decrease and increase of the phase angle at a high frequency range (HF) may be associated with the geometrical effect of the electrochemical cell. As has been reported [25,26], the capacitance of a dielectric layer can be determined by extrapolating the complex-capacitance plots to infinite frequency ($C_\infty$), which does not require the assumption of any specific model and can be determined by fitting the impedance data. Table 3 shows that the $C_\infty$ values increased with time, which indicates decreased oxide resistance related to an increase in the anodic current. Fig. 5(c, d) shows the Bode plots of the T-ArP sample after exposure to a 0.1 M solution of $Na_2SO_4$ at E = OCP. The impedance response also revealed a capacitive loop associated with oxide film formation. The |Z| did not show a significant effect of the Ar-plasma pretreatment, and as can be seen from the phase angle as a function of exposure time plots, CPE behavior was not well defined. The α values were lower than those for the T sample, which decreased with exposure time. The Q coefficient and $C_\infty$ values are not shown in Table 3 because the chi-square goodness of fit was much > 1.

Fig. 6 shows the Bode plots of the T-PMMA and T-ArP-PMMA samples as a function of exposure time to a 0.1 M solution of $Na_2SO_4$ at E = OCP. The impedance results can be described by a general equivalent electrical circuit for coated alloys, as proposed by Epelboin et al. [27]. A capacitive loop is observed in the T-PMMA sample at an early state that is associated with the insulating properties of the PMMA coating. Another capacitive loop was detected in the impedance spectra with more exposure time (Fig. 6(a, b)), which may be attributed to electrolytes penetrating the coating and reaching the metal/coating interface. The $C_\infty$ values for the T-PMMA sample increased slightly with time, as shown in Table 4, suggesting a decrease in coating resistance. Moreover, Fig. 6(a) and Table 4 show that the |Z| of T-PMMA sample in

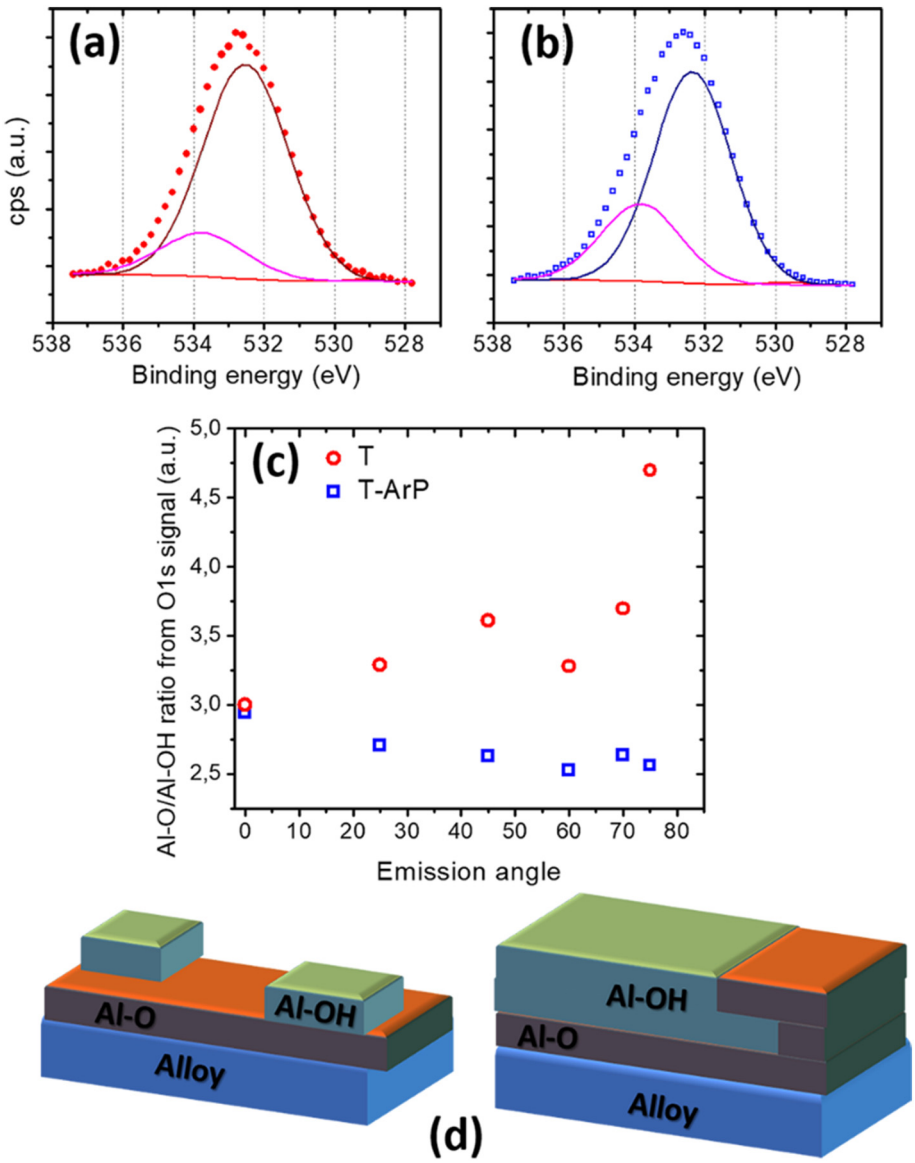


**Fig. 3.** $Al^{3+}/Al^{0}$ XPS-intensity ratios measured at different take-off angle for (a) (○) T and (b) (□) T-ArP samples, (c) reason of the link Al—O and the Al—OH with respect to the angle of emission and (d) representation of the proportions of the Al—OH bond on the surface.

**Table 2**
Characteristics of the types of samples in terms of physical properties: free energy (γ) and polar ($\gamma_S^p$) and dispersive ($\gamma_S^d$) components obtained by static contact angle measurements (θ) in water and diiodomethane.

| System | $\theta_{water}$ (°) | $\theta_{diiodomethane}$ (°) | γ (mN/m) | $\gamma_S^d$ (mN/m) | $\gamma_S^p$ (mN/m) |
|---|---|---|---|---|---|
| T | 56.9 ± 0.1 | 48.5 ± 0.11 | 51.2 | 35.1 | 16.1 |
| T-ArP | 17.7 ± 6.7 | 44.1 ± 1.9 | 75.8 | 38.2 | 37.6 |
| T-PMMA | 78.3 ± 10.1 | 29.1 ± 4.2 | 57.7 | 44.8 | 12.9 |
| T-ArP-PMMA | 86.8 ± 8.8 | 21.1 ± 3.6 | 57.7 | 44.0 | 13.7 |

the LF range decreased with time, from $3.5 \times 10^9\,\Omega\,cm^2$ to $2 \times 10^7\,\Omega\,cm^2$. This concurs with the findings of other publications, including Musiani et al. [26] and Macedo et.al [28]. The impedance response of T-ArP-PMMA sample at medium and LF domain is not incorporated in the graph for shorter exposure time because of the high degree of dispersion of the impedance data in those frequency regions, as shown in Fig. 6(c, d). This suggests an increase in homogeneity of the coatimg due to a higher number of binding sites related to the Ar-plasma pretreatment, which would improve the interaction between PMMA and aluminum surfaces and consequently delay the penetration of the electrolyte in the coating. In fact, the degradation of the coating of the T-ArP-PMMA sample was only observed at day 32 of exposure and, as can be seen in Fig. 6(c), the |Z| value in the LF range was much higher for the T-ArP-PMMA sample than for the T-PMMA sample. This could be attributed to the higher degree of homogenity of the coating, as the contact angle measurements and SEM images suggest [26]. However, a slightly higher $C_\infty$ value was determined for the T-ArP-PMMA sample than for the T-PMMA sample, which suggests more water uptake on the PMMA coating with the Ar-plasma pretreatment, which would keep the water accluded for more time.

Hysteresis angle measurements showed that pretreatment with Ar plasma favors chemical heterogeneity, which in turn increases the hydrophilicity of the coated samples, resulting in lower wettability and a higher hysteresis angle. The electrochemical results showed that pretreatment with Ar-plasma significantly improves the protective capacity of poly (methyl methacrylate) because the obtained coatings are more compact, which slows the penetration of electolytes and better protects the metal against corrosion.

## 4. Conclusions

The Ar-plasma pretreatment modified the surface and interface

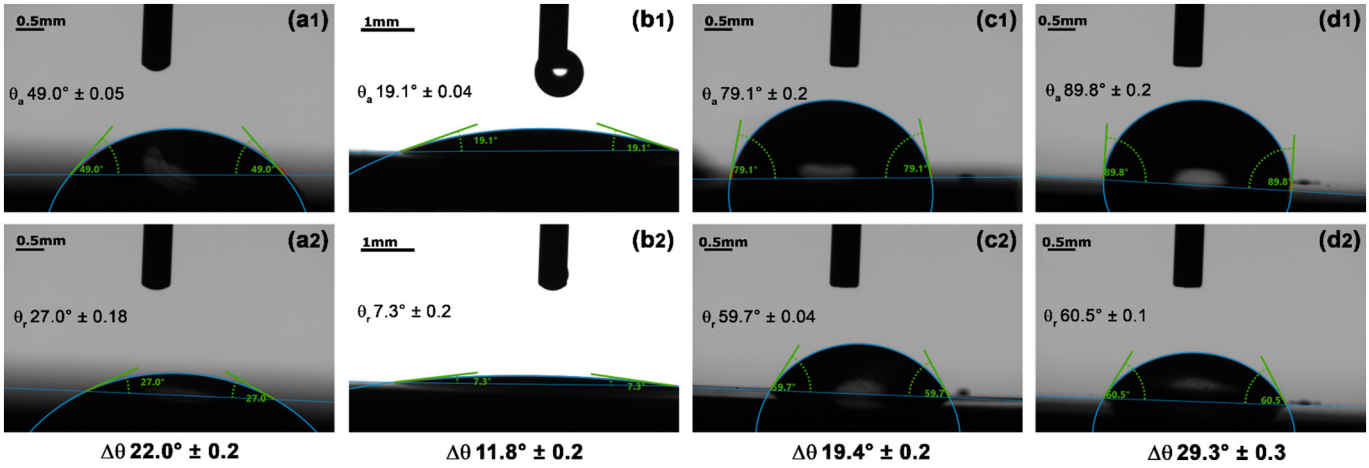


**Fig. 4.** Measurements of the contact angles of advancing ($\theta_a$) and receding ($\theta_r$) and angle of hysteresis in water obtained by: T (a1–a2) T-ArP (b1–b2); T-PMMA (c1–c2) and T-ArP + PMMA (d1–d2).

properties of AA2024. The wettability of the metal surface increased, which was confirmed by contact and hysteresis angles. XPS analysis revealed $Al_2O_3$on the metal surfaces of the Ar-plasma pretreatment samples. This may explain the increase in wettability, and the improved interaction between methoxy groups of the polymer (PMMA) and the hydroxylate aluminum surface, which resulted in more binding sites and increased adhesion, thus improving protection against corrosion. As expected, higher hysteresis angles were estimated, and the impedance modulus was higher after 34 days of exposure. Nevertheless, ionic binding may be more important to the link between aluminum surfaces and PMMA than covalent binding.

**Table 3**
Impedance fit parameters of T and T-ArP samples after exposure to a 0.1 M solution of $Na_2SO_4$.

| System | $t_i$/days | $R_e/\Omega$ | $\lvert Z\rvert_{f=2mHz}/\Omega\,cm^2$ | $\lvert\alpha\rvert$ | $Q/s^{-\alpha}\,cm^2$ | $C_\infty/F\,cm^2$ |
|---|---|---|---|---|---|---|
| T | 1 | 25 | $1.19 \times 10^6$ | 0.86 | $2.09 \times 10^{-6}$ | $0.29 \times 10^{-6}$ |
| T | 7 | 25 | $2.03 \times 10^6$ | 0.87 | $2.73 \times 10^{-6}$ | $2.52 \times 10^{-6}$ |
| T | 15 | 25 | $1.25 \times 10^6$ | 0.89 | $2.69 \times 10^{-6}$ | $3.07 \times 10^{-6}$ |
| T | 32 | 25 | $2.76 \times 10^6$ | 0.89 | $2.76 \times 10^{-6}$ | $6.47 \times 10^{-6}$ |
| T-ArP | 1 | 48 | $4.45 \times 10^5$ | 0.83 | – | – |
| T-ArP | 7 | 50 | $5.95 \times 10^5$ | 0.80 | – | – |
| T-ArP | 15 | 49 | $9.10 \times 10^4$ | 0.71 | – | – |
| T-ArP | 32 | 77 | $7.60 \times 10^5$ | 0.85 | – | – |

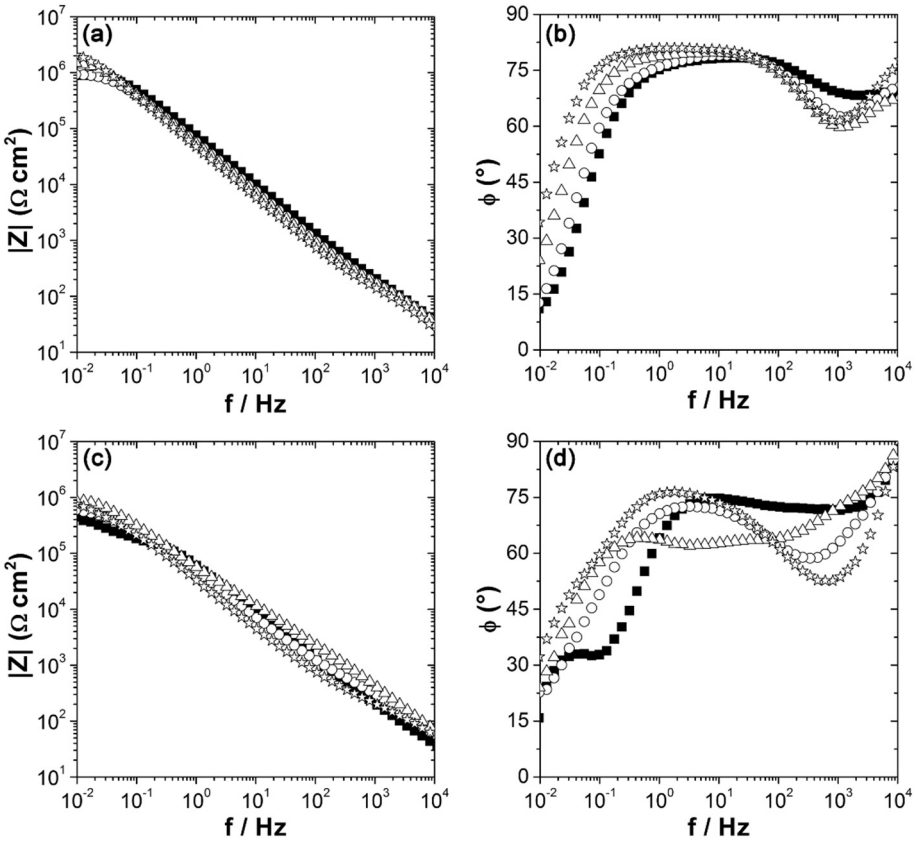


**Fig. 5.** Bode plot of T (a, b) and T-ArP (c, d) samples after exposure to a 0.1 M $Na_2SO_4$ solution obtained at E = OCP. (■) 1 day; (○) 7 days, (Δ) 15 days and (⋆) 32 days.

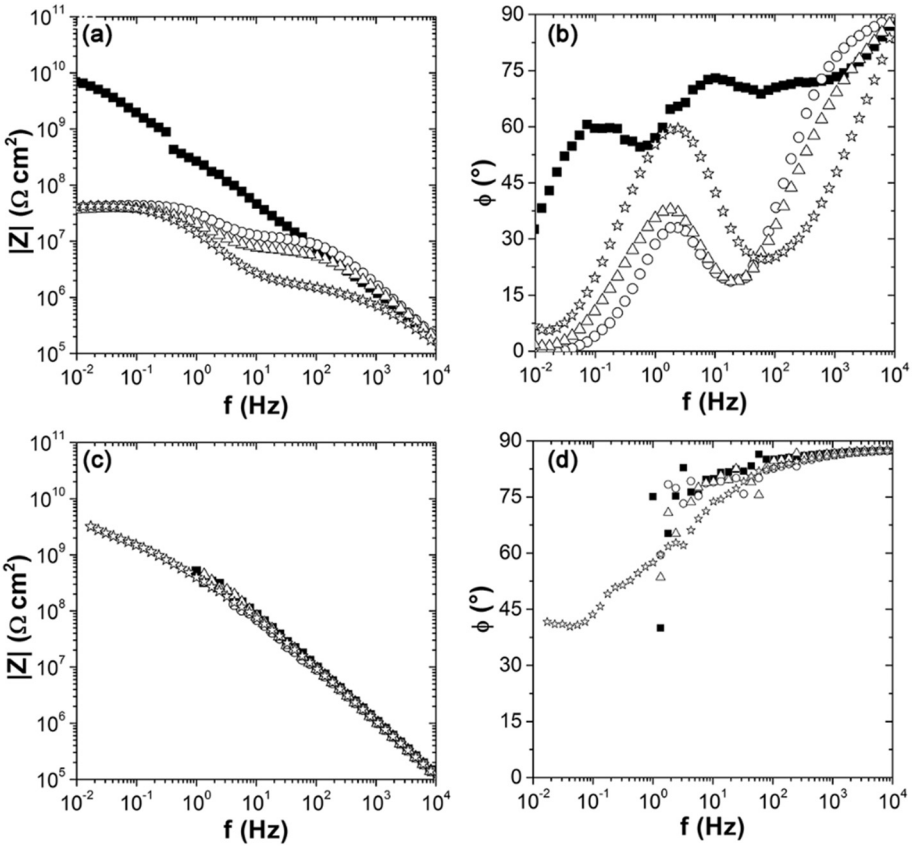


**Fig. 6.** Bode plot of T-PMMA (a, b) and T-ArP-PMMA (c, d) samples after exposure to a 0.1 M $Na_2SO_4$ solution obtained at E = OCP. (■) 1 day; (○) 7 days, (Δ) 15 days and (★) 32 days.

**Table 4**
Impedance parameters of the T-PMMA and T-ArP-PMMA samples after exposure to a 0.1 M solution of $Na_2SO_4$.

| System | $t_i$/days | $C_\infty$/F cm$^2$ | $\lvert Z\rvert_{f\approx 2mHz}$/Ω cm$^2$ |
|---|---|---|---|
| T-PMMA | 1 | $1.56 \times 10^{-10}$ | $3.53 \times 10^9$ |
| T-PMMA | 7 | $1.65 \times 10^{-10}$ | $2.02 \times 10^7$ |
| T-PMMA | 15 | $1.63 \times 10^{-10}$ | $1.90 \times 10^7$ |
| T-PMMA | 32 | $1.71 \times 10^{-10}$ | $2.08 \times 10^7$ |
| T-ArP-PMMA | 32 | $8.46 \times 10^{-10}$ | $5.88 \times 10^9$ |

## Acknowledgements

The authors thank CONICYT (PIA, ACT-1412), FONDECYT (Grants 1160604 and 1180843) and Dicyt-USACH (proyect 051742PC-DAS) for financial support.

## References

[1] P. O'Brien, A. Kortenkamp, The chemistry underlying chromate toxicity, Transit. Met. Chem. 20 (1995) 636–642, https://doi.org/10.1007/BF00136433.
[2] M.W. Kendig, R.G. Buchheit, Corrosion inhibition of aluminum and aluminum alloys by soluble chromates, chromate coatings, and chromate-free coatings, Corrosion 59 (2003) 379–400, https://doi.org/10.5006/1.3277570.
[3] N. Saleema, D.K. Sarkar, R.W. Paynter, D. Gallant, M. Eskandarian, A simple surface treatment and characterization of AA 6061 aluminum alloy surface for adhesive bonding applications, Appl. Surf. Sci. 261 (2012) 742–748, https://doi.org/10.1016/j.apsusc.2012.08.091.
[4] U. Tiringer, J. Kovač, I. Milošev, Effects of mechanical and chemical pre-treatments on the morphology and composition of surfaces of aluminium alloys 7075-T6 and 2024-T3, Corros. Sci. 119 (2017) 46–59, https://doi.org/10.1016/j.corsci.2017.02.018.
[5] L. Domingues, C. Oliveira, J.C.S. Fernandes, M.G.S. Ferreira, EIS on plasma-polymerised coatings used as pre-treatment for aluminium alloys, Electrochim. Acta 47 (2002) 2253–2258, https://doi.org/10.1016/S0013-4686(02)00064-6.
[6] G. Luciano, A. Brinkmann, S. Mahanty, M. Echeverría, Development and evaluation of an eco-friendly hybrid epoxy-silicon coating for the corrosion protection of aluminium alloys, Prog. Org. Coat. 110 (2017) 78–85, https://doi.org/10.1016/j.porgcoat.2017.04.028.
[7] E.M. Liston, L. Martinu, M.R. Wertheimer, Plasma surface modification of polymers for improved adhesion: a critical review, J. Adhes. Sci. Technol. 7 (1993) 1091–1127, https://doi.org/10.1163/156856193X00600.
[8] E.M. Liston, Plasma treatment for improved bonding: a review, J. Adhes. 30 (1989) 199–218, https://doi.org/10.1080/00218468908048206.
[9] T.S.M. Mui, L.L.G. Silva, V. Prysiazhnyi, K.G. Kostov, Surface modification of aluminium alloys by atmospheric pressure plasma treatments for enhancement of their adhesion properties, Surf. Coat. Technol. 312 (2017) 32–36, https://doi.org/10.1016/j.surfcoat.2016.08.024.
[10] E. McCafferty, J.P. Wightman, Determination of the concentration of surface hydroxyl groups on metal oxide films by a quantitative XPS method, Surf. Interface Anal. 26 (1998) 549–564, https://doi.org/10.1002/(SICI)1096-9918(199807)26:8<549::AID-SIA396>3.3.CO;2-H.
[11] E. McCafferty, A surface charge model of corrosion pit initiation and of protection by surface alloying, J. Electrochem. Soc. 146 (1999) 2863, https://doi.org/10.1149/1.1392021.
[12] V. Prysiazhnyi, P. Slavicek, E. Mikmekova, M. Klima, Influence of chemical precleaning on the plasma treatment efficiency of aluminum by RF plasma pencil, Plasma Sci. Technol. 18 (2016) 430–437, https://doi.org/10.1088/1009-0630/18/4/17.
[13] M. Giza, P. Thissen, G. Grundmeier, Adsorption kinetics of organophosphonic acids on plasma-modified oxide-covered aluminum surfaces, Langmuir 24 (2008) 8688–8694, https://doi.org/10.1021/la8000619.
[14] G. Grundmeier, M. Stratmann, Influence of oxygen and argon plasma treatments on the chemical structure and redox state of oxide covered iron, Appl. Surf. Sci. 141 (1999) 43–56, https://doi.org/10.1016/S0169-4332(98)00617-5.
[15] W. Polini, L. Sorrentino, Improving the wettability of 2024 aluminium alloy by means of cold plasma treatment, Appl. Surf. Sci. 214 (2003) 232–242, https://doi.org/10.1016/S0169-4332(03)00359-3.
[16] W. Polini, L. Sorrentino, Adhesion of a protective coating on a surface of aluminium alloy treated by air cold plasma, Int. J. Adhes. Adhes. 27 (2007) 1–8, https://doi.org/10.1016/j.ijadhadh.2005.09.007.
[17] L. Sorrentino, L. Carrino, 2024 aluminium alloy wettability and superficial cleaning improvement by air cold plasma treatment, J. Mater. Process. Technol. 209 (2009) 1400–1409, https://doi.org/10.1016/j.jmatprotec.2008.03.061.
[18] J.C.S. Fernandes, M.G.S. Ferreira, D.B. Haddow, A. Goruppa, R. Short, D.G. Dixon, Plasma-polymerised coatings used as pre-treatement for aluminium alloys, Surf. Coat. Technol. 154 (2002) 8–13, https://doi.org/10.1016/S0257-8972(01)01705-4.
[19] K.H. Kale, A.N. Desaia, Atmospheric pressure plasma treatment of textiles using non-polymerising gases, Indian J. Fibre Text. Res. 36 (2011) 289–299 http://nopr.niscair.res.in/bitstream/123456789/12654/1/IJFTR%2036%283%29%20289-299.pdf.

[20] N. Benito, M. Flores, Evidence of mixed oxide formation on the Cu/$SiO_2$ interface, J. Phys. Chem. C 121 (2017) 18771–18778, https://doi.org/10.1021/acs.jpcc.7b06563.
[21] Q. Liu, X. Tong, G. Zhou, H2O dissociation-induced aluminum oxide growth on oxidized Al(111) surfaces, Langmuir 31 (2015) 13117–13126, https://doi.org/10.1021/acs.langmuir.5b02769.
[22] M. Mrad, Y. Ben Amor, L. Dhouibi, M.F. Montemor, Effect of AA2024-T3 surface pretreatment on the physicochemical properties and the anticorrosion performance of poly(γ-glycidoxypropyltrimethoxysilane) sol-gel coating, Surf. Interface Anal. 50 (2018) 335–345, https://doi.org/10.1002/sia.6373.
[23] J.I. Ahuir-Torres, M.A. Arenas, W. Perrie, G. Dearden, J. de Damborenea, Surface texturing of aluminium alloy AA2024-T3 by picosecond laser: effect on wettability and corrosion properties, Surf. Coat. Technol. 321 (2017) 279–291, https://doi.org/10.1016/j.surfcoat.2017.04.056.
[24] V. Paredes, E. Salvagni, E. Rodriguez, F.J. Gil, J.M. Manero, Assessment and comparison of surface chemical composition and oxide layer modification upon two different activation methods on a cocrmo alloy, J. Mater. Sci. Mater. Med. 25 (2014) 311–320, https://doi.org/10.1007/s10856-013-5083-2.
[25] M. Benoit, C. Bataillon, B. Gwinner, F. Miserque, M.E. Orazem, C.M. Sánchez-Sánchez, B. Tribollet, V. Vivier, Comparison of different methods for measuring the passive film thickness on metals, Electrochim. Acta 201 (2016) 340–347, https://doi.org/10.1016/j.electacta.2015.12.173.
[26] M. Musiani, M.E. Orazem, N. Pébère, B. Tribollet, V. Vivier, Determination of resistivity profiles in anti-corrosion coatings from constant-phase-element parameters, Prog. Org. Coat. 77 (2014) 2076–2083, https://doi.org/10.1016/j.porgcoat.2013.12.013.
[27] L. Beaunier, I. Epelboin, J.C. Lestrade, H. Takenouti, Etude electrochimique, et par microscopie electronique a balayage, du fer recouvert de peinture, Surf. Technol. 4 (1976) 237–254, https://doi.org/10.1016/0376-4583(76)90036-4.
[28] M.C.S.S. Macedo, I.C.P. Margarit-Mattos, F.L. Fragata, J.B. Jorcin, N. Pébère, O.R. Mattos, Contribution to a better understanding of different behaviour patterns observed with organic coatings evaluated by electrochemical impedance spectroscopy, Corros. Sci. 51 (2009) 1322–1327, https://doi.org/10.1016/j.corsci.2009.03.016.